

Néel-Vector-Orientation Induced Intrinsic Half-Metallicity in Two-Dimensional Altermagnets

Xin Chen,¹ Jin Zou,² Lipeng Song,¹ Wei Sun,¹ Yiwen Wu,¹ Luyao Zhu,¹ Xu Cheng,^{3,*} Duo Wang,^{2,†} and Biplab Sanyal^{4,‡}

¹*Thermal Science Research Center, Shandong Institute of Advanced Technology,
Jinan 250100, Shandong Province, People's Republic of China*

²*Faculty of Applied Sciences, Macao Polytechnic University, Macao SAR, 999078, People's Republic of China*

³*Institute for Advanced Technology, Shandong University, Jinan 250061, People's Republic of China*

⁴*Department of Physics and Astronomy, Uppsala University, Box 516, 751 20 Uppsala, Sweden*

(Dated: December 11, 2025)

Whether a zero-moment antiferromagnet can host an intrinsic half-metallic ground state with a single-spin Fermi surface remains an open question in antiferromagnetic spintronics. Existing proposals in compensated magnets reach only transport analogues of this limit and do not realize a genuine AFM half-metallic ground state with a single-spin Fermi surface. Here we show that in two-dimensional altermagnets the Néel-vector orientation acts as an intrinsic knob for magnetic-space-group reduction that lifts the degeneracy between spin sectors. Using Janus monolayer Ta₂TeSeO as a realistic and clean platform and combining symmetry analysis with first-principles calculations, we demonstrate that rotating the Néel vector first breaks the relevant mirror symmetry, opening a gap in one spin sector of symmetry-related Weyl pairs, and then breaks the residual C_{2z} symmetry, shifting the remaining Weyl cones in opposite energy directions so that a single spin sector retains a Fermi surface at the Fermi level. These two symmetry-lowering steps convert a compensated altermagnetic Weyl semimetal into an intrinsic AFM half-metal. The nearly degenerate in-plane magnetic anisotropy then enables reversible switching between the two spin channels using minute strain or weak anisotropic fields. Because this mechanism relies solely on Néel-vector-induced symmetry reduction, it provides a general low-power route to intrinsic half-metallicity in compensated altermagnetic Weyl semimetals.

In condensed-matter physics, simple control knobs such as electric fields or layer stacking angles are widely used to switch materials between qualitatively distinct electronic states. In magnetic systems, the direction of the order parameter is one of the most natural knobs [1–5], routinely used to control anisotropic magnetoresistance or spin-wave spectra. Much less explored is whether reorienting the magnetic order alone, without changing the lattice or composition, can drive a transformation as drastic as turning a compensated antiferromagnet into an antiferromagnetic (AFM) half-metal.

Half-metals, in which one spin channel is metallic while the other is insulating, are central building blocks of spintronic devices because they provide 100% spin-polarized carriers at the Fermi level. All experimentally established half-metals to date, however, are ferro- or ferrimagnetic: spin polarization and net magnetization are tightly locked by broken time-reversal symmetry. From both fundamental and technological perspectives, it is highly desirable to decouple these two quantities and realize a half-metal in a magnetically compensated system. Such an AFM half-metal would simultaneously offer a fully spin-polarized Fermi surface and zero net moment, combining the absence of stray fields, robustness against external perturbations, and ultrafast antiferromagnetic dynamics in a single phase.

The concept of AFM half-metal was introduced by van Leuken and de Groot in 1995 [6], who showed within local-density-approximation calculations that, in principle, fully compensated ferrimagnetic Heusler-type compounds with carefully tuned valence electron counts could combine 100% spin polarization of the conduction electrons with vanishing net magnetization. However, these candidates rely on fine-tuned chemical substitutions and specific crystallographic realizations that have not been confirmed experimentally, and

the mechanism hinges on a delicate cancellation of unequal antiparallel local moments rather than on a symmetry-controlled compensated antiferromagnetic background. As a result, almost three decades after that proposal, no robust intrinsic AFM half-metal has been established in realistic materials. Whether a zero-moment antiferromagnet can host an intrinsic half-metallic ground state with a single-spin Fermi surface therefore remains a central open question in antiferromagnetic spintronics.

Transport analogues of this extreme limit have been proposed in compensated magnets, particularly in altermagnets [7–16], including strain-induced half-semimetallic behavior in Lieb-lattice systems and quasi-one-dimensional compensated spin-filter channels in altermagnetic compounds [17–27]. These scenarios can yield highly spin-polarized transport without net magnetization. However, they still do not realize a genuine AFM half-metallic ground state with a single-spin Fermi surface.

In this work, we demonstrate that such an intrinsic AFM half-metallic state can be realized in a realistic two-dimensional altermagnetic Weyl semimetal. We show that the Néel-vector orientation acts as a symmetry switch that selectively reduces the magnetic space group, gapping out one spin sector via spin-orbit coupling while leaving the other metallic, thereby converting a zero-moment altermagnet into an intrinsic AFM half-metal with a single-spin Fermi surface.

To clarify the underlying mechanism, we revisit standard symmetry operations on axial vectors (magnetic moments) within an orientation-resolved framework in which the Néel vector acts as an intrinsic generator of magnetic space-group (MSG) reduction in altermagnets. Because an axial vector transforms differently from a polar vector under mirror and rotation operations, fixing the magnetic axis converts selected

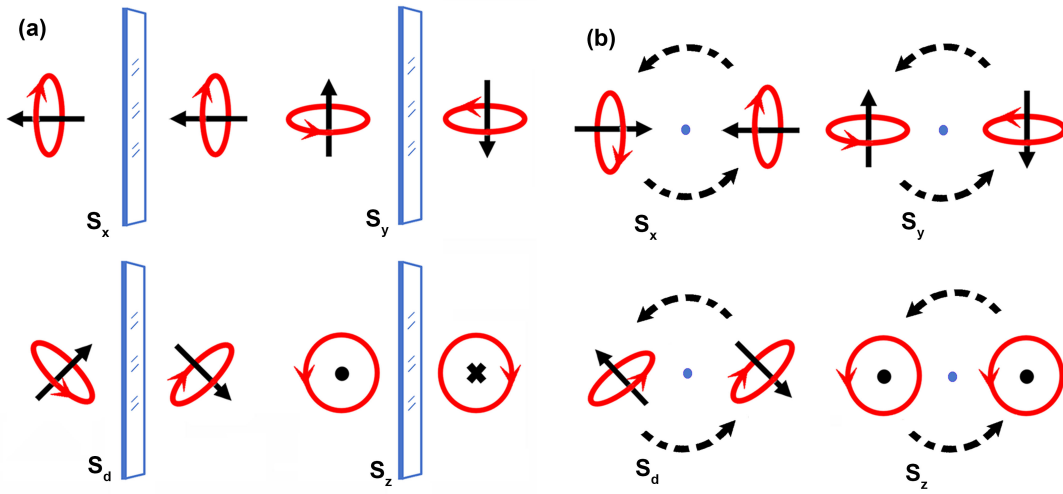


FIG. 1. (a) Mirror-symmetry operation M_x with respect to a plane normal to the x axis applied to magnetic moments for different Néel-vector orientations $\mathbf{n}(x, y, z)$, and $d \equiv (110)$. Black arrows indicate the moment directions, while red circular arrows depict the direction of the equivalent loop current used to visualize the moment, blue lines/rectangles mark the mirror plane. Owing to the axial-vector character of the magnetic moment, M_x leaves the x component unchanged but reverses the components parallel to the mirror plane, i.e., $(m_x, m_y, m_z) \rightarrow (m_x, -m_y, -m_z)$. (b) Rotation-symmetry operation C_{2z} applied to magnetic moments for different Néel-vector orientations $\mathbf{n}(x, y, z)$, and $d \equiv (110)$.

unitary mirrors m into magnetic mirrors $m\mathcal{T}$ or eliminates them entirely. In Lieb and decorated Lieb lattices [19, 26, 28–33] that lack horizontal mirror symmetry M_z and host spin-polarized Weyl points, this Néel-vector-controlled MSG reduction decides which high-symmetry lines retain mirror-protected single-spin crossings and which acquire SOC-allowed mass terms [34]. Monolayer Ta_2TeSeO provides a particularly clean two-dimensional platform for this mechanism: theory predicts giant momentum-dependent spin splitting and spin-polarized, anisotropic Weyl nodes pinned near the Fermi level, as well as nearly degenerate in-plane easy axes along x and y , making Néel-vector rotation energetically inexpensive. Aligning the magnetic axis along the crystallographic x or y direction then breaks M_y or M_x , respectively, and reduces C_{2z} to $C_{2z}\mathcal{T}$, gapping out one spin sector while leaving the other metallic and thereby realizing intrinsic half-metallic states in the altermagnet [35].

Because the magnetic anisotropy on the easy-plane is tiny, minute in-plane strain or weak magnetic fields suffice to reversibly switch the conducting spin channel. The coupling between the lattice and the Néel vector further suggests that circularly polarized light could provide an ultrafast, contact-free control knob [36–38]. The same orientation-controlled symmetry breaking generalizes beyond Ta_2TeSeO and applies even to altermagnets lacking Weyl cones, offering a low-power route to half-metallic transport in compensated systems that complements strain-driven paradigms.

To clarify how the Néel-vector \mathbf{n} orientation affects the surviving magnetic symmetries, we briefly recall the transformation rules of an axial vector under mirror and twofold rotation operations (Fig. 1). In the absence of SOC and without fixing \mathbf{n} , a mirror relates two atoms with the same magnetic moment

and hence enforces their equivalence. Once \mathbf{n} is specified, however, a mirror acts differently on magnetic moment versus polar vectors such as atomic displacement and may no longer relate the two states. The resulting symmetry reduction enables chirality splitting and other C_2 -type anisotropies in the electronic and phonon spectra.

As an example, let the mirror plane be yz (M_x). For an axial vector $\mathbf{S} = (S_x, S_y, S_z)$, the transformation is

$$M_x : (S_x, S_y, S_z) \mapsto (S_x, -S_y, -S_z), \quad (1)$$

where the extra minus sign for the in-plane components originates from $\det M_x = -1$. This is conveniently visualized by the loop-current picture [5] of a magnetic moment in Fig. 1(a): a loop whose normal is along x is unchanged by M_x , while loops with normals along y or z reverse their circulation. Consequently:

- for $\mathbf{n} \parallel x$, the unitary mirror M_x survives;
- for $\mathbf{n} \parallel y$ or z , M_x inverts the moment and must be accompanied by time reversal to be a symmetry (magnetic mirror $M_x\mathcal{T}$);
- for $\mathbf{n} \parallel d \equiv (110)$, M_x maps $d \rightarrow [1\bar{1}0]$, i.e., rotates the in-plane axis by 90° within the layer.

Rotations act on axial and polar vectors identically, so

$$C_{2z} : (S_x, S_y, S_z) \mapsto (-S_x, -S_y, S_z). \quad (2)$$

For an in-plane Néel vector, C_{2z} reverses the moment and must be combined with time reversal to remain a symmetry, thus the composite antiunitary $C_{2z}\mathcal{T}$ is preserved when $\mathbf{n} \perp z$, while it is generally broken for $\mathbf{n} \parallel z$ (because \mathcal{T} flips S_z).

In a Janus decorated Lieb lattice with spin-polarized Weyl points, M_z is naturally broken, M_x and M_y can be selectively broken by an in-plane Néel vector. Combining this with the reduction from the fourfold composite $C_{4z}\mathcal{T}$ to $C_{2z}\mathcal{T}$ when \mathbf{n} is fixed along x or y , two direct and one implied consequences can be concluded:

1. *Weyl-pair in different spin-channel inequivalence.* Nodes related by 90° rotation are no longer symmetry-locked, so they may acquire different energies or gaps.
2. *Weyl-pair in same spin-channel inequivalence.* Nodes related by 180° rotation are no longer symmetry-locked since the mirror symmetry breaking and C_{2z} symmetry breaking, so they may acquire different energies or gaps. This can change semimetal to metal.
3. *Selective gapping and half-metallic.* Symmetry now permits a mass term in one spin sector while forbidding it in the other, leaving one sector gapless with half-metallic dispersion and gapping the opposite sector.

Taken together, the mirror-selection and the $C_{2z}\mathcal{T}$ reduction provide a compact, orientation-resolved mechanism for symmetry-controlled spin-channel selection and chirality splitting, as we will demonstrate explicitly for monolayer Ta_2TeSeO .

Our calculated structure and magnetic configuration of Ta_2TeSeO are shown in Fig. 2(a). The unit cell contains one Se, one Te, one O atom and two antiferromagnetically coupled Ta atoms ($\sim 0.73\mu\text{B}$). Calculated inter-site magnetic exchange parameters and determination of the Néel temperature (346.9 K and 235 K by MFA and classical Monte Carlo simulations, respectively) are given in the Supplementary Materials(SM). The in-plane lattice parameter is about 4.22 Å. All Ta atoms lie in one plane, sandwiched by Se and Te atomic layers, showing a Janus structure. An oxygen atom is situated at the middle atomic plane close to Ta layer, and slightly buckled. In the nonmagnetic limit the monolayer adopts the symmorphic space group $P4mm$ (No. 99), whose point group is C_{4v} generated by C_{4z} and several vertical mirror symmetry. The horizontal mirror M_z is absent due to the Janus polarity. Dynamical stability is confirmed by phonon calculations given in the SM.

In the SOC-free limit, Ta_2TeSeO factorizes into two spin blocks, and each block realizes a pair of symmetry-pinned Weyl cones on the Brillouin-zone boundary. The minimal irreducible high symmetry path and corresponding band structure are shown in Figs. 2 (b) and (d), respectively. The pinning is enforced by unitary in-plane mirrors: along the $M_3 - M_1$ and $M_1 - M_2$ lines, the little group contains M_x and M_y , respectively. Within a single-spin block the two crossing Bloch states transform according to different one-dimensional irreducible representations of the mirror, so the only 2×2 mass term $m\sigma_y$ that could hybridize them [39],

$$H_0(\mathbf{q}) = v_{\parallel}q_{\parallel}\sigma_x + v_{\perp}q_{\perp}\sigma_z, \quad M : \sigma_y \mapsto -\sigma_y, \quad (3)$$

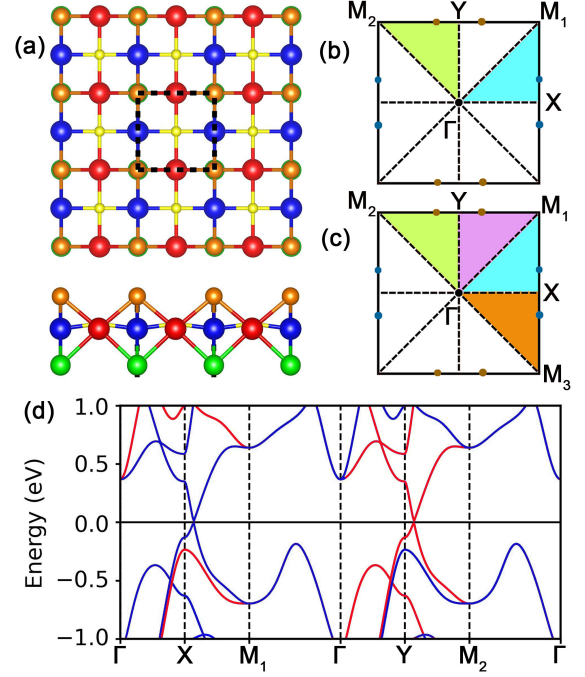


FIG. 2. (a) Top and side views of monolayer Ta_2TeSeO . Yellow, red, blue, orange, and green spheres denote O atoms, spin-up-polarized Ta atoms, and spin-down-polarized Ta atoms, Se atoms, and Te atoms, respectively. (b) The first BZ of Ta_2TeSeO , with all Weyl points are shown. The green and blue areas are the two irreducible parts of the first BZ when SOC effect is not taken into account. (c) The first BZ of Ta_2TeSeO . The four areas in different color are the four irreducible parts of the first BZ when SOC effect is taken into account. (d) The band structure without SOC are shown. The up- and down-spin channels are depicted in red and blue, respectively.

is odd under the corresponding mirror and therefore forbidden by symmetry[40]. This $k \cdot p$ form makes explicit that a mirror-invariant little group excludes the term $m\sigma_y$.

Turning on SOC, $\lambda\mathbf{L} \cdot \mathbf{S}$, couples spin to the crystalline orbital basis, and the AFM order selects a Néel vector \mathbf{n} (an axial vector). Whether the mirror that protected the single-spin Weyl cone survives now depends on \mathbf{n} . Under a reflection M_x (plane yz), an axial vector transforms as $(n_x, n_y, n_z) \mapsto (n_x, -n_y, -n_z)$. Thus, $\mathbf{n} \parallel \hat{x}$ preserves the unitary M_x but breaks M_y . Conversely, $\mathbf{n} \parallel \hat{z}$ breaks both M_x and M_y as unitary symmetries (at most their antiunitary magnetic counterparts $M_{x,y}\mathcal{T}$ remain). The crucial point is that antiunitary operations do not provide a good quantum number that distinguishes the two crossing branches on a mirror-invariant line. Hence, once the corresponding unitary mirror is lost, the hybridization $m\sigma_y$ becomes symmetry-allowed. In an SOC language, the amplitude obeys

$$m(\mathbf{n}) \propto \lambda |n_{\perp}| = \lambda \begin{cases} \sqrt{n_y^2 + n_z^2}, & \text{for breaking } M_x, \\ \sqrt{n_x^2 + n_z^2}, & \text{for breaking } M_y. \end{cases} \quad (4)$$

opening a gap $\Delta = 2|m|$. Thus, by selecting the Néel-axis ori-

entation, one mirror remains unitary and protects the crossing in one spin sector, while the other mirror becomes magnetic (or absent) and permits a gap in the opposite sector, exactly the selective gapping mechanism resolved in Fig. 3.

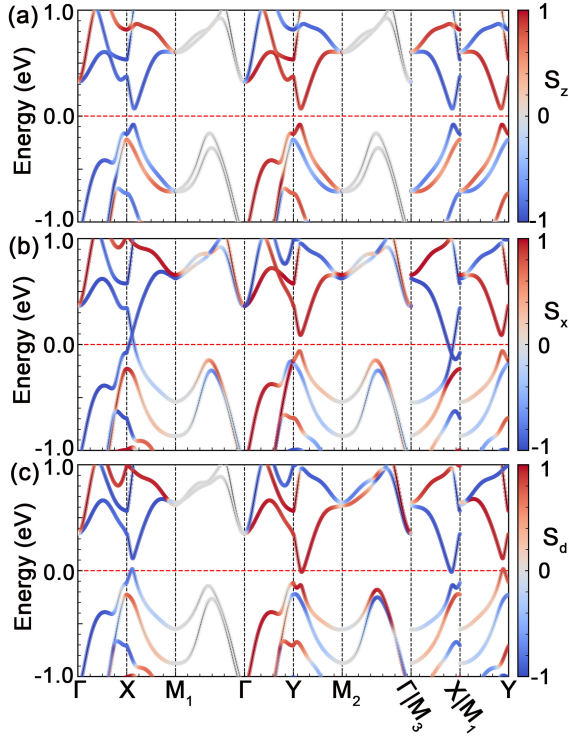


FIG. 3. Spin-projected electronic band structures of Ta_2TeSeO for magnetic axis aligned along (a) the out-of-plane z direction, (b) the in-plane x direction, and (c) the in-plane diagonal (110) direction.

Selective mirror breaking explains why one set of nodes is gapped. What remains to explain is why the other pair of nodes, protected by the surviving mirror, are no longer pinned to the same energy, as shown in Fig. 3(b). The two surviving nodes (on $X-M_1$ and $X-M_3$) cease to be isoenergetic because fixing an in-plane x -direction Néel axis breaks the unitary twofold rotation C_{2z} .

In the parent C_{4v} phase, the two mirror lines $X-M_1$ and $X-M_3$ are related by the unitary twofold rotation C_{2z} : C_{2z} maps $X-M_3$ onto $-X-M_2$, which is equivalent to $X-M_1$ after a reciprocal-lattice translation. This symmetry enforces $E_W^{(1)} = E_W^{(3)}$, where $i = 1 (X-M_1), 3 (X-M_3)$, and hence the equivalence of the two cones. With $\mathbf{n} \perp z$, only the antiunitary $C_{2z}\mathcal{T}$ may remain, it flips spin and imposes no constraint within a fixed spin block, so the nodes along $X-M_1$ and $X-M_3$ can shift to different energies. For the protected spin sector a minimal $k \cdot p$ reads

$$H_i(\mathbf{q}) = v_{i,\parallel} q_{\parallel} \sigma_x + v_{i,\perp} q_{\perp} \sigma_z + m_i \sigma_y + \delta_i \sigma_0. \quad (5)$$

Mirror selection fixes $m_1 = m_3 = 0$ for the protected sector, whereas breaking unitary C_{2z} lifts the constraint $\delta_1 = \delta_3$ and allows independent scalar shifts $\delta_{1,3}$, i.e., $E_W^{(1)} - E_W^{(3)} =$

$\delta_1 - \delta_3 \neq 0$, so the two cones are no longer equivalent. This inequivalence enables the half-semimetal to half-metal conversion: by small symmetry-compatible tuning (strain, gating) one cone is pushed above E_F while the other is pulled below.

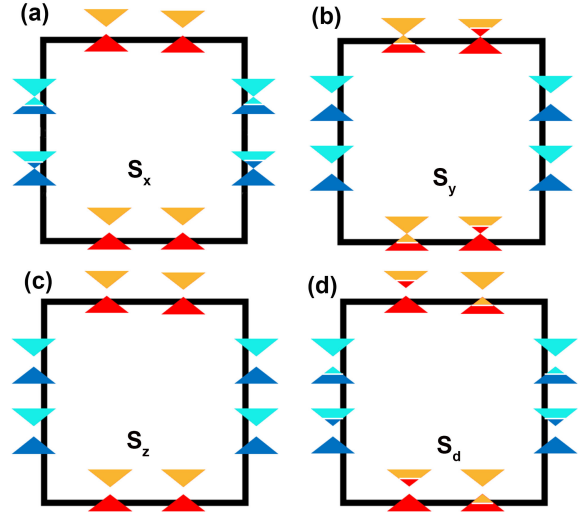


FIG. 4. Symmetry-selected spin-polarized transport under different Néel-vector orientations. Schematic distribution of spin-resolved Weyl cones on the Brillouin-zone boundary when the Néel vector is aligned (a) along x , (b) along y , (c) along z , and (d) along the in-plane diagonal $d \equiv (110)$. Red and orange colors denote the occupied and unoccupied states in spin-up channel, blue and cyan colors denote the occupied and unoccupied in spin-down channel.

The four representative configurations in Fig. 4 illustrate how the Néel-vector orientation governs symmetry and, consequently, the nature of spin-polarized transport. When \mathbf{n} lies along x or y , one in-plane mirror remains unitary while the orthogonal one becomes magnetic, preserving gapless Weyl cones in a single spin channel and producing half-metallic transport with opposite spin polarization for $\mathbf{n} \parallel x$ and $\mathbf{n} \parallel y$. For $\mathbf{n} \parallel z$, both in-plane mirror symmetries are broken but C_{2z} is retained, so both spin sectors open equal gaps, forming a compensated insulating state. For \mathbf{n} along the diagonal $d \equiv (110)$, in-plane mirrors are broken and unitary C_{2z} is also lost, leading to energy-inequivalent gapped states within each spin sector.

In summary, we introduce a Néel-vector-oriented framework for magnetic space-group (MSG) reduction that intrinsically realizes half-metallicity in two-dimensional altermagnets. Using monolayer Ta_2TeSeO as a prototype, we show that without SOC, each spin subspace hosts a pair of mirror-protected Weyl points. Fixing the Néel vector along x (y) preserves the unitary mirror M_x (M_y) while converting its orthogonal partner into a magnetic mirror, allowing a SOC-induced mass term only in one spin sector while keeping the other gapless. Moreover, breaking the unitary C_{2z} symmetry (leaving only $C_{2z}\mathcal{T}$) lifts the equivalence between the two surviving Weyl cones, driving an intrinsic half-semimetal to half-metal transition and producing a single-spin Fermi surface.

We emphasize that this mechanism requires (i) symmetry-enforced altermagnetic Weyl cones near the Fermi energy, (ii) the absence of horizontal mirror symmetry, and (iii) a Néel-vector direction that lowers the magnetic space-group symmetry. This makes monolayer Ta₂TeSeO a fine-tuned yet clean platform and at the same time provides a concrete set of design criteria for future materials searches. Because the in-plane anisotropy is nearly degenerate, minute strain or weak magnetic fields can reversibly switch the conducting spin channel without net magnetization. The same principle generalizes to other two-dimensional decorated Lieb altermagnets satisfying these symmetry conditions (e.g., V₂SeSO, Nb₂SeTeO), offering a symmetry-efficient route to achieve half-metallic transport in compensated systems.

We would like to thank Shandong Institute of Advanced Technology and National Supercomputing Center (Shuguang) for providing computational resources. This work is supported by the National Natural Science Foundation of Shandong Province (Grant No. ZR2024QA040). Xin Chen thanks China scholarship council for financial support (No. 201606220031). Duo Wang acknowledges financial support from the Science and Technology Development Fund from Macau SAR (Grant No. 0062/2023/ITP2 and No. 0016/2025/RIA1) and the Macao Polytechnic University (Grant No. RP/FCA-03/2023). Biplab Sanyal acknowledges financial support from Swedish Research Council (grant no. 2022-04309) and STINT Mobility Grant for Internationalization (grant no. MG2022-9386).

* xchengab@sdu.edu.cn

† duo.wang@mpu.edu.mo

‡ biplab.sanyal@physics.uu.se

- [1] Z. Xiao, J. Zhao, Y. Li, R. Shindou, and Z.-D. Song, Spin space groups: Full classification and applications, *Phys. Rev. X* **14**, 031037 (2024).
- [2] W.-T. Li, Y.-B. Wu, L. Zhuang, J.-T. Wang, and W.-M. Liu, Spin-orbit coupling-driven chirality switching of spin waves in altermagnets (2025), arXiv:2508.18585 [cond-mat.mes-hall].
- [3] H.-J. Duan, M.-S. Fang, M.-X. Deng, and R. Wang, Néel vector and rashba soc effects on rkky interaction in 2d d-wave altermagnets (2025), arXiv:2509.26285 [cond-mat.mes-hall].
- [4] L. Zhiheng, M. Dengpan, C. Jiangtao, X. Yan, and L. Zhifeng, Spin-axis dynamic locking (2025), arXiv:2509.18476 [cond-mat.other].
- [5] Rodríguez-Carvajal, J. and Bourée, F., Symmetry and magnetic structures, *EPJ Web of Conferences* **22**, 00010 (2012).
- [6] H. van Leuken and R. A. de Groot, Half-metallic antiferromagnets, *Phys. Rev. Lett.* **74**, 1171 (1995).
- [7] L. Šmejkal, J. Sinova, and T. Jungwirth, Emerging research landscape of altermagnetism, *Phys. Rev. X* **12**, 040501 (2022).
- [8] L. Šmejkal, J. Sinova, and T. Jungwirth, Beyond conventional ferromagnetism and antiferromagnetism: A phase with nonrelativistic spin and crystal rotation symmetry, *Phys. Rev. X* **12**, 031042 (2022).
- [9] L.-D. Yuan, Z. Wang, J.-W. Luo, E. I. Rashba, and A. Zunger, Giant momentum-dependent spin splitting in centrosymmetric low-*z* antiferromagnets, *Phys. Rev. B* **102**, 014422 (2020).
- [10] L. Šmejkal, R. González-Hernández, T. Jungwirth, and J. Sinova, Crystal time-reversal symmetry breaking and spontaneous hall effect in collinear antiferromagnets, *Sci. Adv.* **6**, eaaz8809 (2020).
- [11] V. Leeb, A. Mook, L. Šmejkal, and J. Knolle, Spontaneous formation of altermagnetism from orbital ordering, *Phys. Rev. Lett.* **132**, 236701 (2024).
- [12] L. Šmejkal, A. B. Hellenes, R. González-Hernández, J. Sinova, and T. Jungwirth, Giant and tunneling magnetoresistance in unconventional collinear antiferromagnets with nonrelativistic spin-momentum coupling, *Phys. Rev. X* **12**, 011028 (2022).
- [13] H. Bai, L. Han, X. Y. Feng, Y. J. Zhou, R. X. Su, Q. Wang, L. Y. Liao, W. X. Zhu, X. Z. Chen, F. Pan, X. L. Fan, and C. Song, Observation of spin splitting torque in a collinear antiferromagnet ruo₂, *Phys. Rev. Lett.* **128**, 197202 (2022).
- [14] T. Jungwirth, R. M. Fernandes, E. Fradkin, A. H. MacDonald, J. Sinova, and L. Šmejkal, Altermagnetism: An unconventional spin-ordered phase of matter, *Newton* **1**, 10.1016/j.newton.2025.100162 (2025), published: 2025-08-04, Accessed: 2025-10-07.
- [15] Y.-P. Zhu, X. Chen, X.-R. Liu, Y. Liu, P. Liu, H. Zha, G. Qu, C. Hong, J. Li, Z. Jiang, X.-M. Ma, Y.-J. Hao, M.-Y. Zhu, W. Liu, M. Zeng, S. Jayaram, M. Lenger, J. Ding, S. Mo, K. Tanaka, M. Arita, Z. Liu, M. Ye, D. Shen, J. Wrachtrup, Y. Huang, R.-H. He, S. Qiao, Q. Liu, and C. Liu, Observation of plaid-like spin splitting in a noncoplanar antiferromagnet, *Nature* **626**, 523 (2024).
- [16] X. Chen, Y. Liu, P. Liu, Y. Yu, J. Ren, J. Li, A. Zhang, and Q. Liu, Unconventional magnons in collinear magnets dictated by spin space groups, *Nature* **640**, 349 (2025).
- [17] S.-J. Gong, C. Gong, Y.-Y. Sun, W.-Y. Tong, C.-G. Duan, J.-H. Chu, and X. Zhang, Electrically induced 2d half-metallic antiferromagnets and spin field effect transistors, *Proceedings of the National Academy of Sciences* **115**, 8511 (2018).
- [18] Y. Liu, S.-D. Guo, Y. Li, and C.-C. Liu, Two-dimensional fully compensated ferrimagnetism, *Phys. Rev. Lett.* **134**, 116703 (2025).
- [19] X. Chen, D. Wang, L. Li, and B. Sanyal, Giant spin-splitting and tunable spin-momentum locked transport in room temperature collinear antiferromagnetic semimetallic CrO monolayer, *Appl. Phys. Lett.* **123**, 022402 (2023).
- [20] L.-D. Yuan, A. B. Georgescu, and J. M. Rondinelli, Nonrelativistic spin splitting at the brillouin zone center in compensated magnets, *Phys. Rev. Lett.* **133**, 216701 (2024).
- [21] X. Li and J. Yang, First-principles design of spintronics materials, *Natl. Sci. Rev.* **3**, 365 (2016).
- [22] X. Hu, Half-metallic antiferromagnet as a prospective material for spintronics, *Adv. Mater.* **24**, 294 (2012).
- [23] S.-D. Guo, Y. Liu, J. Yu, and C.-C. Liu, Valley polarization in twisted altermagnetism, *Phys. Rev. B* **110**, L220402 (2024).
- [24] S.-D. Guo, Valley polarization in two-dimensional zero-net-magnetization magnets, *Applied Physics Letters* **126**, 080502 (2025).
- [25] B. Wu, Y.-l. Song, W.-x. Ji, P.-j. Wang, S.-f. Zhang, and C.-w. Zhang, Quantum anomalous hall effect in an antiferromagnetic monolayer of moo, *Phys. Rev. B* **107**, 214419 (2023).
- [26] J.-Y. Li, A.-D. Fan, Y.-K. Wang, Y. Zhang, and S. Li, Strain-induced valley polarization, topological states, and piezomagnetism in two-dimensional altermagnetic v2te2o, v2steo, v2sseo, and v2s2o, *Applied Physics Letters* **125**, 222404 (2024).
- [27] J. Tian, J. Li, H. Liu, Y. Li, Z. Liu, L. Li, J. Li, G. Liu, and J. Shi, Spin-layer coupling in an altermagnetic multilayer: A design

- principle for spintronics, *Phys. Rev. B* **111**, 035437 (2025).
- [28] H.-Y. Ma, M. Hu, N. Li, J. Liu, W. Yao, J.-F. Jia, and J. Liu, Multifunctional antiferromagnetic materials with giant piezomagnetism and noncollinear spin current, *Nature Communications* **12**, 2846 (2021).
- [29] X. Xu and L. Yang, Altermagnets in two-dimensional lattice magnets, *Nano Letters* **25**, 11870 (2025).
- [30] Y. Che, H. Lv, X. Wu, and J. Yang, Engineering altermagnetic states in two-dimensional square tessellations, *Phys. Rev. Lett.* **135**, 036701 (2025).
- [31] W. Xie, X. Xu, Y. Yue, H. Xia, and H. Wang, Piezovoltage effect and magnetovoltage coupling in altermagnetic semiconductors studied by first-principles calculations, *Phys. Rev. B* **111**, 134429 (2025).
- [32] Y. Jiang, X. Zhang, H. Bai, Y. Tian, B. Zhang, W.-J. Gong, and X. Kong, Strain-engineering spin-valley locking effect in altermagnetic monolayer with multipiezoelectric properties, *Applied Physics Letters* **126**, 053102 (2025).
- [33] I. Khan, D. Bezzerga, B. Marfoua, and J. Hong, Altermagnetism, piezovoltage, and ferroelectricity in two-dimensional Cr₂SeO altermagnet, *npj 2D Materials and Applications* **9**, 18 (2025).
- [34] X.-Q. Sun, S.-C. Zhang, and T. c. v. Bzdušek, Conversion rules for weyl points and nodal lines in topological media, *Phys. Rev. Lett.* **121**, 106402 (2018).
- [35] A. A. Zyuzin, S. Wu, and A. A. Burkov, Weyl semimetal with broken time reversal and inversion symmetries, *Phys. Rev. B* **85**, 165110 (2012).
- [36] H. Ueda, M. García-Fernández, S. Agrestini, C. P. Romao, J. van den Brink, N. A. Spaldin, K.-J. Zhou, and U. Staub, Chiral phonons in quartz probed by x-rays, *Nature* **618**, 946 (2023).
- [37] M. Che, J. Liang, Y. Cui, H. Li, B. Lu, W. Sang, X. Li, X. Dong, L. Zhao, S. Zhang, T. Sun, W. Jiang, E. Liu, F. Jin, T. Zhang, and L. Yang, Magnetic order induced chiral phonons in a ferromagnetic weyl semimetal, *Phys. Rev. Lett.* **134**, 196906 (2025).
- [38] S. Chaudhary, D. M. Juraschek, M. Rodriguez-Vega, and G. A. Fiete, Giant effective magnetic moments of chiral phonons from orbit-lattice coupling, *Phys. Rev. B* **110**, 094401 (2024).
- [39] T. H. Hsieh, H. Lin, J. Liu, W. Duan, A. Bansil, and L. Fu, Topological crystalline insulators in the same material class, *Nature Communications* **3**, 982 (2012).
- [40] J. Liu, W. Duan, and L. Fu, Two types of surface states in topological crystalline insulators, *Phys. Rev. B* **88**, 241303 (2013).